Quantifying the impact of dust on heterogeneous ice generation in midlevel supercooled stratiform clouds

Damao Zhang,[1] Zhien Wang,[1,2] Andrew Heymsfield,[3] Jiwen Fan,[4] Dong Liu,[2] and Ming Zhao[5]

Received 21 June 2012; revised 10 August 2012; accepted 19 August 2012; published 26 September 2012.

[1] Dust aerosols have been regarded as effective ice nuclei (IN), but large uncertainties regarding their efficiencies remain. Here, four years of collocated CALIPSO and CloudSat measurements are used to quantify the impact of dust on heterogeneous ice generation in midlevel supercooled stratiform clouds (MSSCs) over the 'dust belt'. The results show that the dusty MSSCs have an up to 20% higher mixed-phase cloud occurrence, up to 8 dBZ higher mean maximum Z_e (Z_e_max), and up to 11.5 g/m^2 higher ice water path (IWP) than similar MSSCs under background aerosol conditions. Assuming similar ice growth and fallout history in similar MSSCs, the significant differences in Z_e_max between dusty and non-dusty MSSCs reflect ice particle number concentration differences. Therefore, observed Z_e_max differences indicate that dust could enhance ice particle concentration in MSSCs by a factor of 2 to 6 at temperatures colder than −12°C. The enhancements are strongly dependent on the cloud top temperature, large dust particle concentration and chemical compositions. These results imply an important role of dust particles in modifying mixed-phase cloud properties globally.
Citation: Zhang, D., Z. Wang, A. Heymsfield, J. Fan, D. Liu, and M. Zhao (2012), Quantifying the impact of dust on heterogeneous ice generation in midlevel supercooled stratiform clouds, *Geophys. Res. Lett.*, *39*, L18805, doi:10.1029/2012GL052831.

1. Introduction

[2] Heterogeneous ice nucleation is critical for precipitation and to Earths' radiation budget, but it still is poorly understood because of the largely unknown properties of aerosol particles that serve as ice nuclei (IN) and catalyze the ice nucleation process [*Cantrell and Heymsfield*, 2005]. Dust particles have been widely recognized as efficient IN and as one of the major IN sources from various remote sensing observations [*Seifert et al.*, 2010], field campaigns [*DeMott et al.*, 2010] and laboratory measurements [*Hoose and Möhler*, 2012]. Model simulations also show that ice particle number concentrations in mixed-phase clouds are largely impacted by the compositions and size distributions of dust particles [*Eidhammer et al.*, 2009]. Although the major dust source regions are located over the 'dust belt', including the North Africa, the Arabian Peninsula and East Asia [*Liu et al.*, 2008], dust particles can be ejected into the free troposphere and transported around the globe; thus, these dust particles have a global impact [*Yang et al.*, 2012]. Therefore, understanding the impact of dust on ice generation plays an important role in disentangling the complicated relationships between aerosols and IN concentrations in clouds.

[3] However, there are large uncertainties in our current understanding of the efficiency of dust as IN. Previous laboratory studies showed that the onset conditions for dust particles acting as IN are strongly dependent on the mineralogy, size or surface area of the particles, surface coating, and nucleation mode [*Hoose and Möhler*, 2012]. *Sassen et al.* [2003] reported the glaciation of supercooled altocumulus clouds by long-range transported African dust particles at temperatures as warm as ∼−5°C based on lidar measurements in southern Florida. On the other hand, with lidar measurements close to the dust source regions, *Ansmann et al.* [2008] showed that no ice formation was observed in supercooled stratiform clouds with cloud-top temperatures warmer than −18°C. Our limited understanding is also reflected by differences of up to 4 orders of magnitude in dust freezing fractions as reported in several published IN parameterizations [*Phillips et al.*, 2008]. Thus, more observations are needed to understand and resolve these uncertainties. Thus far, observations of the impacts of dust on ice generation on a global scale are still scarce, and no IN parameterizations used in current climate models have been developed or evaluated using satellite measurements. In this letter, we present a quantitative estimation of the impact of dust on ice generation in midlevel supercooled stratiform clouds (MSSCs) over the 'dust belt' by employing four years of collocated CALIPSO and CloudSat measurements.

2. Identification of Dusty MSSCs Using CloudSat and CALIPSO Measurements

[4] The Cloud–Aerosol Lidar with Orthogonal Polarization (CALIOP) on the CALIPSO satellite was the first spaceborne polarization lidar, providing total attenuated backscattering (TAB) coefficient profiles at the wavelengths of 532 nm and 1064 nm. CALIOP also provides the linear depolarization ratio at 532 nm, with vertical resolutions of 30 m below 8.2 km and 60 m between 8.2 and 20.2 km [*Winker et al.*, 2009]. *Liu et al.* [2008] demonstrated that the height of the dust layer top and bottom can be determined using the CALIOP TAB and depolarization ratio for cloud-free profiles. Due to the strong daytime noise levels in CALIOP measurements, only nighttime measurements are used for dust detection in this study.

[1]Department of Atmospheric Science, University of Wyoming, Laramie, Wyoming, USA.
[2]Hefei Institutes of Physical Science, Chinese Academy of Sciences, Hefei, China.
[3]National Center for Atmospheric Research, Boulder, Colorado, USA.
[4]Pacific Northwest National Laboratory, Richland, Washington, USA.
[5]SimCenter Enterprises, Inc., Chattanooga, Tennessee, USA.

Corresponding author: Z. Wang, Department of Atmospheric Science, University of Wyoming, 1000 E. University Ave., Laramie, WY 82071-2000, USA. (zwang@uwyo.edu)

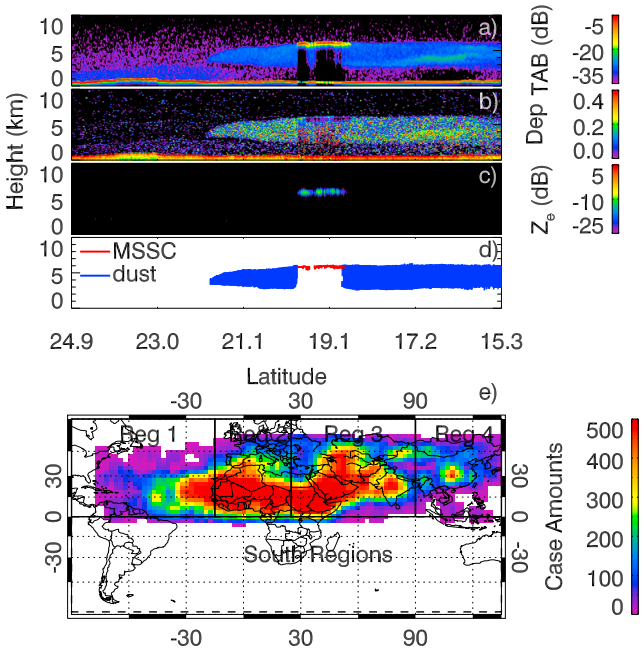

Figure 1. An example of dusty MSSC: (a) CALIOP TAB profiles at 532 nm; (b) CALIOP depolarization profiles at 532 nm; (c) CloudSat CPR radar reflectivity profiles; (d) identified dust layers and MSSC; (e) global distribution of dusty MSSCs in terms of numbers of profiles in 2.5° × 2.5°grid boxes from four years of collocated CALIPSO/ CloudSat measurements.

[5] CloudSat carried the first spaceborne cloud radar - a 94.05 GHz Cloud Profiling Radar - to provide radar reflectivity factor (Z_e) profiles with a vertical resolution of 500 m [*Stephens et al.*, 2008]. The close flying formation of CloudSat and CALIPSO provides almost simultaneous radar and lidar measurements globally [*Stephens et al.*, 2008]. As illustrated by *Zhang et al.* [2010], the collocated CALIPSO and CloudSat measurements provide a unique dataset to globally detect MSSCs and ice generation within them. Overall, the MSSCs cover approximately 7.8% of Earth's surface, and 83.3% of MSSCs with cloud top temperatures colder than 0°C are in the mixed-phase on global average [*Zhang et al.*, 2010]. MSSCs represent a "natural laboratory" for studying ice generation in clouds because of their less-complex dynamic environments and well-defined vertical thermodynamic structure [*Fleishauer et al.*, 2002]. A thin, supercooled liquid-dominated (in both concentration and water content) mixed-phase layer (usually less than ~500 m) is generally located at the upper part of MSSCs, and falling ice crystals are located below [*Wang et al.*, 2004].

[6] These MSSCs can form in the elevated dense dust layer, as in the case shown in Figure 1, offering a great opportunity to evaluate the impact of dust acting as IN on ice generation in MSSCs. CALIOP generally cannot penetrate the liquid water-dominated layer at the top of the MSSCs to detect the dust layer or the ice below clouds, unlike ground-based lidar measurements [*Wang et al.*, 2004]. Therefore, we must rely on the dust layer being detected between clouds or surrounding clouds to infer whether MSSCs are affected by dust particle. If dust layers are detected near either one side or both sides of an MSSC system and the dust layers extend up to the height of the MSSC layer, this MSSC layer is considered to be affected by dust particles and is referred to a dusty MSSC. Figures 1a–1d present a dusty MSSC case with a cloud top at ~6 km and a temperature of ~−10°C. Based on the CALIPSO measurements, given in Figures 1a and 1b, elevated dust layers are detected on both sides of MSSCs [*Liu et al.*, 2008], with the top and bottom layers located at approximately 6 km and 3 km, respectively. CloudSat Z_e measurements, given in Figure 1c, show conspicuous ice virga below the mixed-phase layer.

[7] Four years of collocated CALIPSO level 1 and CloudSat 2B-GEOPROF data from the period of June 2006 to May 2010 are analyzed in this study. In addition, ancillary state variable data (e.g., temperature, pressure) from the European Center for Medium-Range Weather Forecasts provided in the ECMWRF-AUX product are used to provide Cloud Top Temperature (CTT) values. To avoid the seeding effect and the attenuation of the lidar signal from the upper layers, we only include single layer cloud cases by removing multiple cloud layer cases using the CloudSat 2B-GEOPROF-LIDAR product. In total, ~6.3×10^5 dusty MSSC profiles are identified. Figure 1e shows the geographical distribution of these dusty MSSCs in terms of numbers of profiles within a 2.5° × 2.5° grid box. The dusty MSSCs are mainly located in the region of latitudes between 0N and 45N and longitudes between 75W and 135E. Approximately, 3.5×10^6 non-dusty MSSC profiles in the same region are identified.

[8] Dust particles from different source regions may have different ice nucleating abilities because of their different chemical compositions and size distributions [*Formenti et al.*, 2011]. Therefore, the dusty MSSCs are separated into four sub-regions for further analyses based on the regional source of the dust and the transported distance, as indicated in Figure 1e. Region 1 represents long-range transported dust, which might be coated with soluble materials during the transportation and have reduced IN capability [*Eastwood et al.*, 2009]. The dust particles in region 2 and region 3 are near both the Saharan and Saudi Arabian dust source regions. Dust particles in region 4 are transported over eastern China from the Gobi desert and may interact with pollutant aerosols, which could change their dust ice nucleating ability [*Formenti et al.*, 2011]. Non-dusty MSSCs in the 'dust belt' might still be influenced by background dust particles that are difficult to detect by CALIOP. Therefore, we also include MSSCs in the same longitude and latitude ranges in the Southern Hemisphere for comparison. These areas are referred to as the 'South Regions' (Figure 1e). In total, ~2.6×10^6 'South Regions' MSSC profiles are identified.

3. Results and Discussions

[9] Due to the weak updrafts and turbulence in MSSCs, ice crystals are primarily formed in the upper part of the supercooled cloud layer, due to the region's colder temperature, grow large in a water-saturated environment and fall out of the mixed-phase layer [*Wang et al.*, 2004]. Below the liquid-dominated mixed-phase cloud layer, ice crystals continue to grow and fall until they reach the level below the ice-saturation condition. This simple ice generation and growth pattern in MSSCs offers opportunities to use Z_e measurements to quantitatively infer the ice concentration. Under similar meteorological conditions in terms of CTT and liquid water path (LWP), ice crystal growths in MSSCs are expected to be statistically identical.

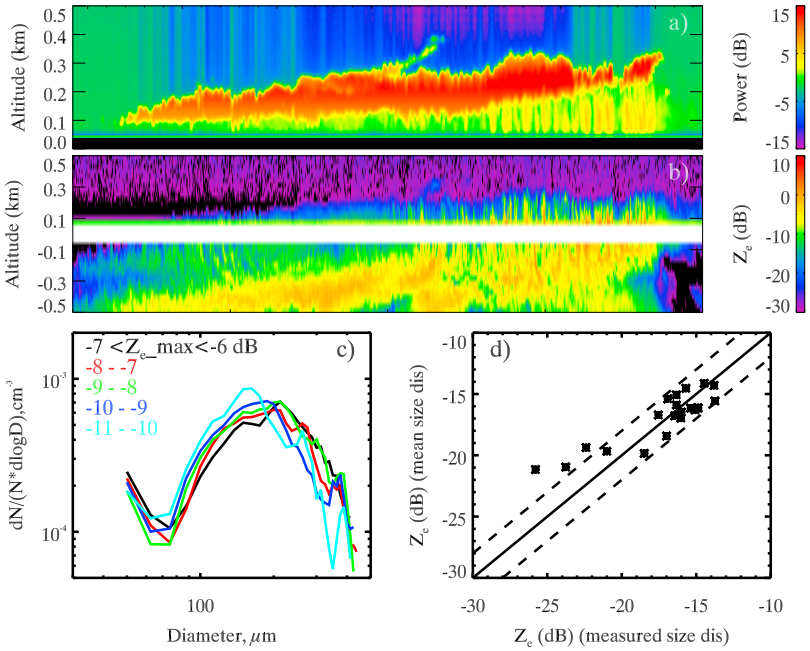

Figure 2. (a) A MSSC system detected by WCL during ICE-L on December 10th, 2007, the lidar power is uncalibrated attenuated backscattering; (b) Z_e structure from WCR and the white line in the middle indicating aircraft level; (c) normalized ice particle size distributions from 2D-C measurements and binned with Z_e_max; (d) calculated Z_e using measured ice particle size distributions and mean normalized ice particle size distribution. The dashed lines are ±2 dB lines.

[10] Figure 2 provides an airborne observation case to support this argument. The integrated remote sensing and *in situ* sampling capability of the C-130 during the Ice in Clouds Experiment-Layer clouds (ICE-L) [*Heymsfield et al.*, 2011] offered collocated Z_e and ice size distribution measurements. Wyoming Cloud Lidar (WCL) and Wyoming Cloud Radar (WCR) measurements (Figures 2a and 2b) show a typical MSSC we are interested in and the aircraft flew below the clouds to measure ice crystal size distributions. Figure 2c shows that all ice particle size distributions normalized by the correspondent total ice concentration and binned with Z_e_max were similar to each other. Figure 2d compares Z_e calculated using measured particle size distributions and the mean normalized particle size distribution, with the same total concentration. It indicates that usage of the same normalized size distribution in this MSSC only causes approximately 0.3 dB biases of Z_e, with a standard deviation of 1.7 dB. There are few data points with more than 2 dB differences, which could be caused by the lower LWP compared with the rest of the cloud. Considering possible fluctuations caused by small 2D-C sampling volume, this case confirms that it is appropriate to assume the same ice distribution shape for similar MSSCs.

[11] This means that the maximum Z_e (Z_e_max) within 500 m of the MSSC cloud top contains ice crystal concentration information. Thus, we can use differences in Z_e_max among similar MSSCs to evaluate the relative magnitudes of the impact of dust on ice generation in MSSCs. Due to existing issues in retrieving LWP in mixed-phase clouds from space, the maximum TAB was then used as a proxy to select clouds with similar LWPs under a given CTT. To ensure that cases with a narrow TAB range were used and to simultaneously obtain enough samples, the TAB range was chosen around the peak of the TAB probability distribution, which is between 0.31–0.45 sr^{-1} km^{-1}.

[12] Figures 3a–3c show the occurrence of MSSCs in terms of CTT and Z_e_max within the selected narrow TAB range. Note that the occurrence is normalized in each temperature bin. Ice particles begin to occur in MSSCs at CTT of ∼−7°C based on the Z_e thresholds [*Zhang et al.*, 2010]. However, at temperatures warmer than −10°C, Z_e_max might also be affected by supercooled drizzles near the cloud top [*Rasmussen et al.*, 2002], but it is less likely a problem for these MSSCs because they are geometrically thin [*Fleishauer et al.*, 2002]. When ice particles are detected based on the Z_e thresholds, the MSSC is regarded as being in a mixed-phase state. The mixed-phase fractions, defined as the fractions of ice containing MSSCs to all MSSCs, increase with decreasing CTT for all three groups, as shown in Figure 3d. The mixed-phase fractions for 'South Regions' compare pretty well with those from *Seifert et al.* [2010], while the dusty and non-dusty cases have higher mixed-phase fractions than those from *Seifert et al.* [2010] at each CTT. This confirms the strong dependence of ice generation on the CTT. There are sharp increases of the mixed-phase MSSC fractions begin at ∼−10°C, suggesting that significant ice generation starts at this temperature in MSSCs, which is also consistent with laboratory measurements (R. M. Rasmussen, personal communication, 2011). Generally, the dusty MSSCs have up to ∼20% higher mixed-phase fractions at CTTs colder than −10°C, indicating that dusty MSSCs are more likely to produce ice particles under similar meteorological conditions, which is consistent with long-term ground-based observations [*Seifert et al.*, 2010]. Approximately 98% of dusty MSSCs are in the mixed-phase

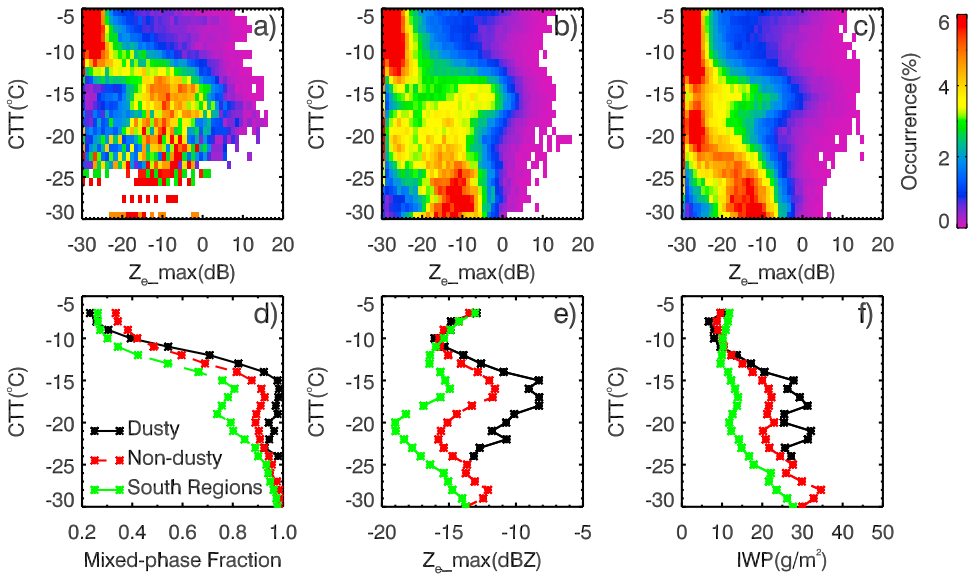

Figure 3. (a) The occurrence of dusty MSSCs in terms of CTT and Z_e_max within the TAB value of 0.31–0.45 (sr^{-1} km^{-1}); (b) for non-dusty MSSCs; (c) for 'South Regions' MSSCs. (d) Mean mixed-phase occurrence at given CTT for dusty, non-dusty and 'South Regions' MSSCs. (e) Same as Figure 3d, but for the mean Z_e_max of mixed-phase MSSCs. (f) Same as Figure 3d, but for the mean IWP of mixed-phase MSSCs.

when the cloud top temperature was ∼−15°C, while the non-dusty and 'South Region' cases only reach this magnitude of mixed-phase fraction below a CTT of ∼−30°C (Figure 3d). However, the supercooled liquid cloud layers (without detectable ice) could persist down to temperatures as low as −30°C, especially in the 'South Regions'.

[13] Statistically, Z_e_max increases sharply starting from ∼−10°C, reaches its peak at ∼−15°C, and then begin to decrease until reaching a CTT of ∼−20°C for all three groups; this feature is more obvious for the mean Z_e_max in Figure 3e. In addition to the temperature-dependent ice concentration, this Z_e_max pattern is also affected by the temperature dependency of the ice diffusional growth rate [*Sulia and Harrington*, 2011]. The local minima of mean Z_e_max at ∼−10°C and ∼−20°C are caused by the slow growth of an isometric habit, and the maximum mean Z_e_max at ∼−15°C corresponded to the rapid growth of dendritic habit. For the 'South Regions' and non-dusty cases, the increasing mean Z_e_max as CTT decreases from ∼−20°C reflects the general behavior of increasing ice number concentration as temperatures decrease due to slow ice growth at colder temperatures [*Sulia and Harrington*, 2011]. For each group, MSSCs have a wide range of Z_e_max at a given CCT, which could be due to different ice concentrations linked to different aerosols or the different life stages of MSSCs. However, the systematically higher mean Z_e_max for dusty cases relative to the other two groups indicates that dust contributes to the high ice concentrations in MSSCs under similar meteorological conditions, as further discussed below.

[14] The strong ice generation in dusty MSSCs results in higher ice water paths (IWPs), as observed in Figure 3f. The cloud IWP is calculated by integrating the ice water content, which is derived from an empirical, temperature-dependent ice water content (IWC)-Z_e relationship [*Hogan et al.*, 2006], from the radar-detected cloud top to its base. Although random errors of IWCs from the relationship could be large, the statistic mean errors are small and similar for the three groups of MSSCs. The IWP increases significantly with decreasing CTT for three groups. The mean IWPs of dusty MSSCs are statistically larger than those of the non-dusty and 'South Regions' cases when the CTT was colder than −12°C. Overall, the mean IWP for the dusty, non-dusty and 'South Regions' cases are 23.4, 19.7 and 11.9 g/m^2, respectively, which means that the mean IWP for dusty MSSCs is ∼19% higher than that of the non-dusty cases and ∼97% higher than that of the 'South Regions' cases. The 3.7 g/m^2 increase of IWP between dusty and non-dusty and 11.5 g/m^2 increase between the dusty and 'South Regions' MSSCs could cause a significant change in the cloud radiative forcing (CRF), based on the previous studies [*DeMott et al.*, 2010].

[15] Figure 4a shows the differences of Z_e_max (dZ_e_max) between dusty and non-dusty and between dusty and 'South Regions' MSSCs, which increase with decreasing CTT until ∼−20°C and then start to decrease. At ∼−20°C, the dusty MSSCs have mean a Z_e_max that is approximately 4 dBZ higher than non-dusty MSSCs in the same region and up to 8 dBZ higher than the 'South Regions' MSSCs. Considering

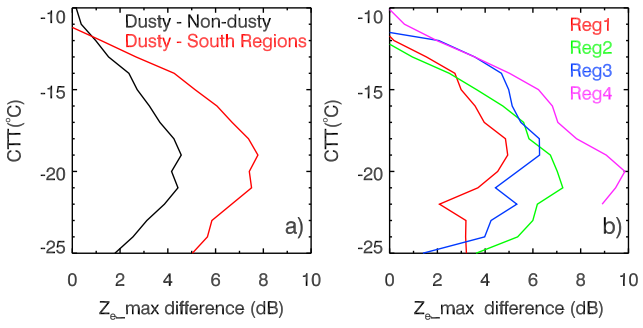

Figure 4. (a) Z_e_max differences between dusty, non-dusty and 'South Regions' MSSCs in terms of CTT. (b) Z_e_max differences between dust and 'South Regions' MSSCs for the four sub-regions as shown in Figure 1e.

a statistically similar ice crystal growth history for similar MSSCs, it is fair to assume that ice concentration is the main cause for the Z_e_max difference. For similar MSSCs, Z_e can be expressed as: Z_e (dBZ) = $10*\log_{10}(N*Z_{e\_nor})$, where N is the total number concentration, Z_{e_nor} is the radar reflectivity factor (mm^6/m^3) for the normalized ice crystal size distribution at the given CTT and LWP. Therefore, an 8-dBZ Z_e_max difference indicates that dust can enhance the ice concentration in MSSCs by a factor of up to 6. With a 2- to 6-fold increase in the mixed-phase cloud ice concentration, the liquid water droplets will be depleted quickly and cause the cloud more likely to glaciate according to previous modeling studies [*Fan et al.*, 2009]. Considering similar or higher dust concentrations at warmer temperatures, the decreasing Z_e_max difference indicates that the effectiveness of dust acting as IN decreases as the CTT increases when the CTT is warmer than −20°C. For MSSCs with a CTT colder than −20°C, the Z_e_max differences decrease as the CTT decreases. This could be a result of decreasing dust concentration with height and/or increasing IN effectiveness of background aerosols at cold temperatures.

[16] Figure 4b shows noticeable variations of the Z_e_max differences between dusty and 'South Regions' MSSCS among the four sub-regions. The Z_e_max differences for region 1 are the smallest, while for the region 4 are the largest. Two possible factors might contribute to these variations of the Z_e_max differences among the four sub-regions. First, the dust concentrations, especially large dust particle concentrations (e.g., with diameter >0.5 μm), are different at the same temperature over the four sub-regions. Indeed, our preliminary analysis shows that, at given temperature (warmer than −25°C), dust particles in region 4 have larger TAB and color ratios (TAB_{1064}/TAB_{532}) than in the other three regions, which indicates higher large dust particle concentrations in region 4. Estimations of large dust particle concentrations from CALIPSO lidar TAB and color ratio measurements are being developed and will be used to quantify dust concentration differences based on the variations of the Z_e_max differences among different regions. A second possible cause of the variations of the Z_e_max differences is due to the possible difference in dust chemical compositions. The mineralogical compositions of dust from the African and Asian source regions are different. For example, the mass ratio of Illite, which is one of the main components of dust and is also the most efficient IN among all the dust components [*Pinti et al.*, 2012], to Kaolinite is generally higher in dust from Asia than that from Africa [*Formenti et al.*, 2011]. *Eastwood et al.* [2009] also showed that the ice-nucleating ability of dust particles is deactivated when they are coated with soluble materials after long-range transportation, as is the case in region 1.

4. Summary

[17] Four years of collocated CALIPSO lidar and CloudSat radar measurements are used to quantitatively estimate the impact of dust on heterogeneous ice generation in MSSCs. This large dataset provides robust evidence that statistically supports the assertion that dust particles are efficient IN at temperatures colder than −10°C. We show that dusty MSSCs are more likely to produce ice particles and contain an up to 20% higher mixed-phase cloud occurrence under similar meteorological conditions. Dusty MSSCs also have a higher IWP of up to 11.5 g/m^2 than that of the 'South Regions' cases, which could result in a significant change of the cloud radiative forcing of MSSCs'. Because the Z_e_max differences among similar MSSCs primarily reflect the ice particle number concentration differences, observed Z_e_max differences indicate that dust can enhance ice concentration in MSSCs by a factor of 2 to 6, compared with background aerosol conditions. The ice concentration enhancements are strongly dependent on the CTT and dust particle properties, such as their size and chemical compositions. Our ongoing studies are refining an approach using CloudSat and CALIPSO measurements to better determine dust concentrations and correlate them with the ice generation in MSSCs. Because of the high sensitivities of liquid-phase properties in mixed-phase clouds on IN concentration, these results indicate that reliable simulations of dust impacts on ice generation in climate models are critical to capturing aerosol-cloud-radiation-dynamics feedback.

[18] **Acknowledgments.** This research was funded by NASA grant NNX10AN18G, and also partially supported by DOE DE-SC0006974 as part of the ASR program. We thank CALIPSO PI Dave Winker, CloudSat PI Graeme Stephens and the CALIPSO and CloudSat data group. We are grateful for the comments from two anonymous reviewers.

[19] The Editor thanks two anonymous reviewers for assisting in the evaluation of this paper.

References

Ansmann, A., et al. (2008), Influence of Saharan dust on cloud glaciation in southern Morocco during the Saharan Mineral Dust Experiment, *J. Geophys. Res.*, *113*, D04210, doi:10.1029/2007JD008785.

Cantrell, W., and A. Heymsfield (2005), Production of ice in tropospheric clouds: A review, *Bull. Am. Meteorol. Soc.*, *86*, 795–807, doi:10.1175/BAMS-86-6-795.

DeMott, P. J., et al. (2010), Predicting global atmospheric ice nuclei distributions and their impacts on climate, *Proc. Natl. Acad. Sci. U. S. A.*, *107*, 11,217–11,222, doi:10.1073/pnas.0910818107.

Eastwood, M. L., S. Cremel, M. Wheeler, B. J. Murray, E. Girard, and A. K. Bertram (2009), Effects of sulfuric acid and ammonium sulfate coatings on the ice nucleation properties of kaolinite particles, *Geophys. Res. Lett.*, *36*, L02811, doi:10.1029/2008GL035997.

Eidhammer, T., P. J. DeMott, and S. M. Kreidenweis (2009), A comparison of heterogeneous ice nucleation parameterizations using a parcel model framework, *J. Geophys. Res.*, *114*, D06202, doi:10.1029/2008JD011095.

Fan, J., M. Ovtchinnikov, J. M. Comstock, S. A. McFarlane, and A. Khain (2009), Ice formation in Arctic mixed-phase clouds: Insights from a 3-D cloud-resolving model with size-resolved aerosol and cloud microphysics, *J. Geophys. Res.*, *114*, D04205, doi:10.1029/2008JD010782.

Fleishauer, R. P., V. E. Larson, and T. H. Vonder Haar (2002), Observed microphysical structure of midlevel, mixed-phase clouds, *J. Atmos. Sci.*, *59*, 1779–1804, doi:10.1175/1520-0469(2002)059<1779:OMSOMM>2.0.CO;2.

Formenti, P., et al. (2011), Recent progress in understanding physical and chemical properties of African and Asian mineral dust, *Atmos. Chem. Phys.*, *11*, 8231–8256, doi:10.5194/acp-11-8231-2011.

Heymsfield, A. J., et al. (2011), Ice in clouds experiment—Layer clouds. Part I: Ice growth rates derived from lenticular wave cloud penetrations, *J. Atmos. Sci.*, *68*, 2628–2654, doi:10.1175/JAS-D-11-025.1.

Hogan, R. J., M. P. Mittermaier, and A. J. Illingworth (2006), The retrieval of ice water content from radar reflectivity factor and temperature and its use in evaluating a mesoscale model, *J. Appl. Meteorol. Climatol.*, *45*, 301–317, doi:10.1175/JAM2340.1.

Hoose, C., and O. Möhler (2012), Heterogeneous ice nucleation on atmospheric aerosols: A review of results from laboratory experiments, *Atmos. Chem. Phys. Discuss.*, *12*, 12,531–12,621, doi:10.5194/acpd-12-12531-2012.

Liu, D., Z. Wang, Z. Liu, D. Winker, and C. Trepte (2008), A height resolved global view of dust aerosols from the first year CALIPSO lidar measurements, *J. Geophys. Res.*, *113*, D16214, doi:10.1029/2007JD009776.

Phillips, V. T. J., P. J. DeMott, and C. Andronache (2008), An empirical parameterization of heterogeneous ice nucleation for multiple chemical species of aerosol, *J. Atmos. Sci.*, *65*, 2757–2783, doi:10.1175/2007JAS2546.1.

Pinti, V., C. Marcolli, B. Zobrist, C. R. Hoyle, and T. Peter (2012), Ice nucleation efficiency of clay minerals in the immersion mode, *Atmos. Chem. Phys. Discuss.*, *12*, 3213–3261, doi:10.5194/acpd-12-3213-2012.

Rasmussen, R. M., I. Geresdi, G. Thompson, K. Manning, and E. Karplus (2002), Freezing drizzle formation in stably stratified layer clouds: The role of radiative cooling of cloud droplets, cloud condensation nuclei, and ice initiation, *J. Atmos. Sci.*, *59*, 837–860, doi:10.1175/1520-0469(2002)059<0837:FDFISS>2.0.CO;2.

Sassen, K., P. J. DeMott, J. M. Prospero, and M. R. Poellot (2003), Saharan dust storms and indirect aerosol effects on clouds: CRYSTAL-FACE results, *Geophys. Res. Lett.*, *30*(12), 1633, doi:10.1029/2003GL017371.

Seifert, P., et al. (2010), Saharan dust and heterogeneous ice formation: Eleven years of cloud observations at a central European EARLINET site, *J. Geophys. Res.*, *115*, D20201, doi:10.1029/2009JD013222.

Stephens, G. L., et al. (2008), The CloudSat Mission: Performance and early science after the first year of operation, *J. Geophys. Res.*, *113*, D00A18, doi:10.1029/2008JD009982.

Sulia, K. J., and J. Y. Harrington (2011), Ice aspect ratio influences on mixed-phase clouds: Impacts on phase partitioning in parcel models, *J. Geophys. Res.*, *116*, D21309, doi:10.1029/2011JD016298.

Wang, Z., K. D. Sassen, N. Whiteman, and B. D. Demoz (2004), Studying altocumulus with ice virga using ground-based active and passive remote sensors, *J. Appl. Meteorol.*, *43*, 449–460, doi:10.1175/1520-0450(2004)043<0449:SAWIVU>2.0.CO;2.

Winker, D. M., et al. (2009), Overview of the CALIPSO mission and CALIOP data processing algorithms, *J. Atmos. Oceanic Technol.*, *26*, 2310–2323, doi:10.1175/2009JTECHA1281.1.

Yang, W., A. Marshak, T. Várnai, O. V. Kalashnikova, and A. B. Kostinski (2012), CALIPSO observations of transatlantic dust: vertical stratification and effect of clouds, *Atmos. Chem. Phys. Discuss.*, *12*, 12,051–12,080, doi:10.5194/acpd-12-12051-2012.

Zhang, D., Z. Wang, and D. Liu (2010), A global view of midlevel liquid-layer topped stratiform cloud distribution and phase partition from CALIPSO and CloudSat measurements, *J. Geophys. Res.*, *115*, D00H13, doi:10.1029/2009JD012143.